Research Article Vol. 15, No. 1 / 1 Jan 2024 / Biomedical Optics Express 277
Biomedical Optics EXPRESS

Effect of chronic kidney disease induced calcification on peripheral vascular perfusion using near-infrared spectroscopic imaging

DANIELA LEIZAOLA,[1,3] VALENTINA DARGAM,[2] KEVIN LEIVA,[1] HANIYEH ALIREZAEI,[1] JOSHUA HUTCHESON,[2] AND ANURADHA GODAVARTY[1,*]

[1] *Optical Imaging Laboratory, Biomedical Engineering Department, 10555 W Flagler St, Miami, FL 33174, USA*
[2] *Cardiovascular Matrix Remodeling Laboratory, Biomedical Engineering Department, 10555 W Flagler St, Miami, FL 33174, USA*
[3] *dleiz001@fiu.edu*
[*] *godavart@fiu.edu*

Abstract: Low-cost techniques that can detect the presence of vascular calcification (VC) in chronic kidney disease (CKD) patients could improve clinical outcomes. In this study, we established a near-infrared spectroscopy-based imaging technique to determine changes in peripheral hemodynamics due to CKD-induced VC. Mice were fed a high-adenine diet with either normal or high levels of phosphate to induce CKD with and without VC, respectively. The mice tail was imaged to evaluate hemodynamic changes in response to occlusion. The rate of change in oxyhemoglobin in response to occlusion showed a statistically significant difference in the presence of VC in the mice.

1. Introduction

Chronic kidney disease (CKD) is characterized by irreversible damage to the kidneys typically caused by elevated blood pressure or diabetes. CKD comorbidities include anemia (reduced red blood cells), bone disease (disrupted hormonal function), and cardiovascular disease (CVD). The leading cause of death in CKD patients is CVD, where vascular calcification (VC) is the strongest predictor for CKD-associated cardiovascular risk [1]. CKD patients with no detectable VC have an 8-year all-cause survival rate of ~90% compared to 50% survivability in age-matched patients with medial calcification [2]. Medial calcification reduces vascular wall elasticity, thus increasing cardiac afterload [3,4]. Intimal calcification can promote atherosclerotic plaque rupture, the most common cause of heart attacks [5].

1.1. Peripheral vascular disease in CKD

Peripheral vascular dysfunction and VC in peripheral beds can also occur in CKD patients, which can eventually lead to limb ischemia and amputation [6,7]. The prevalence of amputations worldwide is increasing and is more present in populations from lower social economic status [8,9]. Additionally, assessment of peripheral vascular dysfunction is not commonly performed until a patient requires revascularization procedures or amputation [9,10]. There is a need to better monitor peripheral perfusion in patients with CKD to improve clinical outcomes and prevent amputations.

Once significant calcification develops, it is unclear whether mineral deposition can be reversed. Ongoing clinical studies seek to mitigate VC in early stages of CKD with a goal of improving cardiovascular outcomes [11,12]. The clinical realization of therapeutic approaches will require strategies to detect early signs of vascular remodeling and identify high-risk patients. The gold

#503667 https://doi.org/10.1364/BOE.503667
Journal © 2024 Received 24 Aug 2023; revised 24 Oct 2023; accepted 19 Nov 2023; published 18 Dec 2023

Biomedical Optics EXPRESS

standard for detecting VC relies on contrast-enhanced cardiac computed tomography-based imaging, which requires a contrast agent to detect and quantify coronary calcium. This technique is not well-suited for longitudinal monitoring of vascular calcification due to lack of access, associated expenses, and inherent radiation risks [13]. In particular, limited access to diagnostic tools due to socioeconomic inequalities can lead to underdiagnosis in underserved populations, resulting in significant health disparities in CKD management and poorer outcomes [14]. To address health disparities and enable the advent of anti-calcification therapeutics, there is a need for a low-cost non-invasive approach to accurately screen for indicators of VC in primary care settings or community clinics.

1.2. Low-cost technologies to image blood perfusion

Low-cost techniques that assess peripheral vascular dysfunction can potentially replace expensive imaging modalities. Peripheral perfusion (or microcirculation) assessment can be performed using various non-invasive techniques such as hyperspectral imaging (HSI), Laser-Doppler perfusion imaging (LDPI), laser speckle contrast imaging (LSCI), Near-infrared (NIR) spectroscopy (NIRS), transcutaneous oxygenation measurements ($TcPO_2$) and vascular optical tomography imaging [15]. While $TcPO_2$ is a gold-standard approach, it is time-consuming and has >10% intra-operator variability [15]. On the contrary, the other techniques are near real-time, but no specific indicators have been developed to assess peripheral vascular issues related to calcification. We recently developed a low-cost non-contact near-infrared optical scanner (NIROS) that is capable of spatio-temporal mapping for tissue oxygenation and perfusion in tissues [16,17]. Unlike LDPI that maps for dynamically changing perfusion (but at a single point location), our NIRS approach can obtain these near-real-time perfusion maps across a wide-field region of the imaged peripheries. These near real-time spatio-temporal maps of perfusion changes in the peripheries can be used to develop indicators for flow restrictions with the onset of vascular calcification. NIRS has extensively been used in PAD diagnosis studies to measure oxygen saturation in the muscles at single point location via exercise stimulating protocols [18]. However, these low-cost NIRS devices applied to date are limited to muscle perfusion at point locations, making the approach subjective and inconsistent when applied across patients. The spatio-temporal maps obtained from our NIRS imaging approach measures dynamically changing perfusion at the peripheries—not at single point locations but the entire region of interest, which can reduce subjectivity when clinically applied.

In this pilot study, we applied a non-contact, non-invasive spatio-temporal NIRS based imaging technique to assess whether the onset of CKD-induced VC affects peripheral perfusion of mice. We performed a longitudinal analysis of peripheral blood reperfusion in response to vascular occlusion of the mouse's tail throughout the development of CKD-induced VC.

2. Methodology

2.1. Mouse model

Study protocols were performed on C57BL/6J mice bred at the Florida International University Animal Care Facility and all procedures were approved by the Institutional Animal Care and Use Committee. Adult (10-weeks-old) mice (n = 12) were placed on a high (0.2%) adenine and normal phosphate (0.6%) diet to induce CKD [19]. At week 6, the mice were subdivided in two groups. The control group (CKD, n = 6) was maintained on the high adenine and normal phosphate diet for an additional 6 weeks. The test group (CKD + VC, n = 5) was kept on the high adenine diet supplemented with high phosphate (1.8%) to induce VC [19,20]. In the CKD + VC group, the onset of VC occurs at the start of the high phosphate diet, which has been extensively reported [19,20].

Biomedical Optics EXPRESS

2.2. Instrumentation

A near-infrared optical scanner (NIROS), an in-house NIRs device, was used to image mouse tails for dynamic tissue oxygenation measurements [17]. Tail occlusions were induced using a commercially available tail occlusion cuff and hardware (CODA Monitor, KENT Scientific).

2.2.1. NIROS:

The continuous wave, NIROS was developed to evaluate effective peripheral tissue oxygenation [16,21]. Non-contact imaging was performed to acquire spatio-temporal maps of the mouse tail, with the LED-based source light (at 682 nm and 826 nm wavelengths) multiplexed at a frequency of 2 Hz (1 Hz per respective wavelength). The NIR-sensitive CMOS camera captured the diffuse reflected NIR intensity signals as it passed through a 645 nm long pass filter. Hemoglobin-based parameters were obtained from the diffuse reflected NIR signals by applying a modified Beer-Lambert's law, as described in section 2.4.2.

2.2.2. CODA monitor – noninvasive blood pressure system:

A blood occlusion stimulus was applied on the mouse tail during the imaging session to analyze changes in effective oxygenation of the area. The CODA monitor system by KENT Scientific is a blood-pressure monitoring system for small animal studies that determines blood pressure (BP) using a volumetric pressure cuff (VPR-cuff) and occlusion cuff (O-Cuff). The VPR-cuff was not utilized during the study due to the sensor interfering with a large area of the tail; therefore, solely the and O-Cuff was used. Since the CODA monitor was designed to determine blood pressure with the VPR-cuff and O-Cuff, blood pressure could not be recorded simultaneous to the imaging. The occlusion cycle settings on the CODA monitor allowed control of the release time (15s or 30s) after reaching maximum pressure (~250 mm Hg), and the rest time (45s or 60s) before the next occlusion cycle. In our study, the data analysis was based on the first occlusion cycle and hence it was independent of the release and rest times used during the study.

2.3. Imaging protocol

2.3.1. Study timeline:

Parameters measured during this study include: spatio-temporal NIR diffuse reflectance maps and weight (g) of each mouse. Data was recorded throughout disease progression at the following timepoints: week 0 (weight only), week 6 (baseline), week 9, and week 12 (Fig. 1).

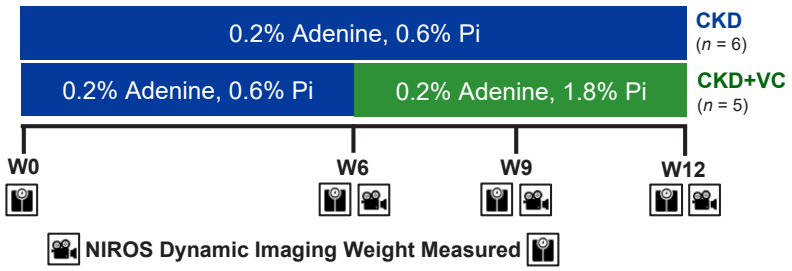

Fig. 1. Study timeline of the diets used to induce CKD and CKD + VC in mice and timepoint of recordings. CKD group without VC was fed a 0.2% Adenine diet (blue) with normal (0.6%) phosphate for 12 weeks. CKD + VC group was fed the same diet for the first 6 weeks and supplemented at week 6 with high (1.8%) phosphate (green). Weight and NIROS dynamic imaging data of mice were acquired during each session at the specified timepoints.

Biomedical Optics EXPRESS

2.3.2. Imaging set-up:

The imaging setup (Fig. 2(A)) and protocol remained constant for both mice groups (n = 11) and across all sessions. NIROS was secured onto the procedure table, positioned 120 mm from imaging surface (heating pad for body temperature stability), such that the field of view would encompass the entire tail. The mice were anesthetized in a chamber using isoflurane (isoflurane 1–2%, oxygen 1–3%) [22], and placed on the imaging surface in a dorsal position (Fig. 2(B)). During the imaging session, isoflurane anesthetic was maintained on the mouse via nose cone and adjusted accordingly by visual observation of breath rate. A fiducial marker was placed below the tail, proximal to the body, for analysis of tail area post-image acquisition (Fig. 2(B)).

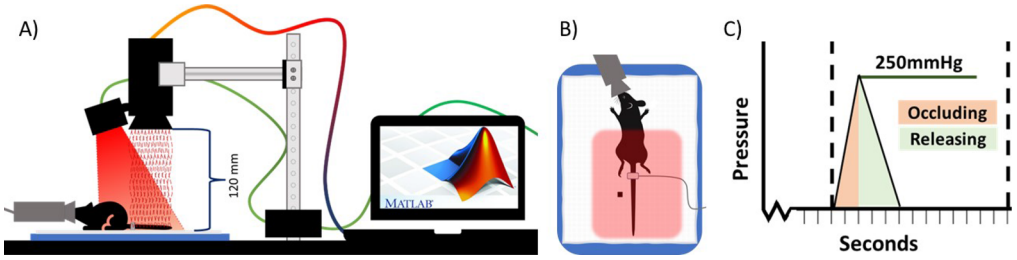

Fig. 2. Imaging protocol A) NIROS setup fixed above the mouse and parallel to the imaging surface. B) Anesthetized mouse placed in prone position with occlusion cuff on the tail, near the body. NIROS imaging area depicted by the red rectangular area. C) Representative image of an occlusion cuff cycle that reaches maximum pressure of 250 mmHg rapidly to occlude the tail (10-12s) and then releases gradually (15s).

The Kent Scientific CODA monitor was calibrated at the start of each imaging session as specified by the manual. Only the O-cuff was used during the imaging session, and it was placed at the base of the tail proximal to the body (Fig. 2(B)).

NIROS imaging was conducted for a total of 10 minutes: 5 minutes of imaging prior to and without an occlusion stimulus (rest) followed by 5 minutes of imaging with the occlusion stimulus (occlusion). The initial period (rest, 5-minutes) was considered a stabilization period for the mouse's body temperature to reach the heat pad temperature and deep anesthesia. The stabilization period was followed by the occlusion cycles (for, 5 minutes), in which the occlusion cuff reached maximum pressure (250 mmHg) within 10-12 seconds (Fig. 2(C)) and the pressure release time was 15 seconds. Several occlusion cycles were recorded; however, data analysis in this study focused only on the first occlusion cycle during each imaging session.

2.4. Data analysis

2.4.1. Hemoglobin-based parameter analysis:

Hemoglobin-based parameters (oxy- [ΔHbO], deoxy- [ΔHbR], and total hemoglobin [ΔHbT]) were determined by a Modified Beer-Lambert's law (MBLL). Diffuse reflectance maps recorded using NIROS (Fig. 3(A)) were used to calculate spatio-temporal maps of the effective hemoglobin-based parameters by changes in the optical density at each wavelength per timepoint, and pixel location, (Eq. (1)) [17]. The effect of dark noise (I_D) was considered for each corresponding pixel intensity value ($I_{t=n}$). A calibration image ($I_{0,\ t=n}$) was taken at the start of each imaging session as an indicator of a highly diffusive surface.

$$\Delta OD_{t=n}(x, y, \lambda_i) = -\log_{10}\left(\frac{I_{t=n}(\lambda_i, x, y) - I_D(x, y)}{I_{0,\ t=n}(\lambda_i, x, y) - I_D(x, y)}\right) \tag{1}$$

The spatio-temporal optical density maps at each wavelength was, in turn, used along with molar extinction coefficients of [HbO] ($\varepsilon^{\lambda}_{HbO}$) and [$HbR$] ($\varepsilon^{\lambda}_{HbR}$) at the respective wavelengths as

Biomedical Optics EXPRESS

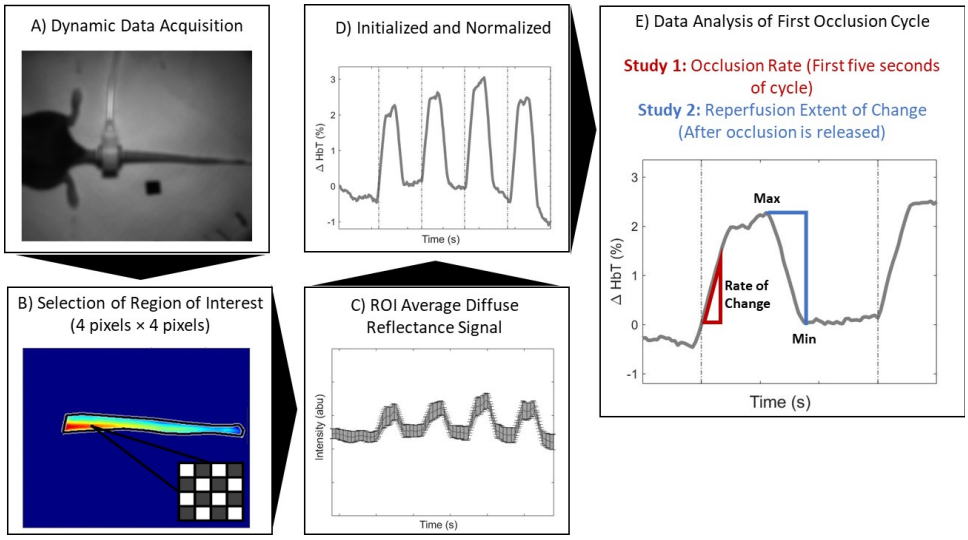

Fig. 3. Flowchart of effective hemoglobin-based parameter and indicator extraction with respect to time. Analysis was completed for each mouse for the respective imaging session. A) NIROS diffuse reflectance image showing field of view that includes the mouse tail, occlusion cuff and fiducial marker. B) Mean intensity map of the hemoglobin-based parameter across time on the mouse's tail. A region of interest was chosen on the vessel, determined by color bar intensity. C) Average of the hemoglobin-based parameter's intensity trendlines for the chosen region of interest with respect to the time with mean error. D) Normalization of hemoglobin-based parameter (ΔHbT is shown) with respect to 60 seconds prior to the start of the first occlusion. E) Calculation of two indicators during the first occlusion cycle for comparison: rate of change (during occlusion) and extent of change.

given in Eq. (2) and Eq. (3).

$$[HbO](x,y,t) = \frac{(\varepsilon_{HbR}^{\lambda 1}\Delta OD^{\lambda 2}) - (\varepsilon_{HbR}^{\lambda 2}\Delta OD^{\lambda 1})}{[(\varepsilon_{HbR}^{\lambda 1}\varepsilon_{HbO}^{\lambda 2}) - (\varepsilon_{HbR}^{\lambda 2}\varepsilon_{HbO}^{\lambda 1})]LB} \tag{2}$$

$$[HbR](x,y,t) = \frac{(\varepsilon_{HbO}^{\lambda 2}\Delta OD^{\lambda 1}) - (\varepsilon_{HbO}^{\lambda 1}\Delta OD^{\lambda 2})}{[(\varepsilon_{HbR}^{\lambda 1}\varepsilon_{HbO}^{\lambda 2}) - (\varepsilon_{HbR}^{\lambda 2}\varepsilon_{HbO}^{\lambda 1})]LB} \tag{3}$$

L (inter-optode distance) and B (path length factor) are assumed to not change with respect to time or wavelength, thus are grouped to obtain the effective spatio-temporal maps of $[\Delta HbO]$ (Eq. 4) and $\Delta HbR]$ (Eq. 5).

$$[\Delta HbO](x,y,t) = [HbO](x,y,t)LB \tag{4}$$

$$[\Delta HbR](x,y,t) = [HbR](x,y,t)LB \tag{5}$$

The effective total hemoglobin (ΔHbT) was calculated by the summation of the effective concentration of oxy-hemoglobin $[\Delta HbO]$ and deoxy-hemoglobin $[\Delta HbR]$ within the chosen ROI prior to further calculations. And the oxygen saturation $[\Delta StO_2]$ was calculated as the ratio of $[\Delta HbO\,]/[\,\Delta HbT]$.

$$[\Delta HbT](x,y,t) = [\Delta HbO](x,y,t) + [\Delta HbR](x,y,t) \tag{6}$$

In this study, effective spatio-temporal hemoglobin parameters were utilized across time to analyze the dynamic changes in response to the occlusion stimulus on the mouse's tail. A flow

Biomedical Optics EXPRESS

chart of the data analysis process is given in Fig. 3. The tail region to be analyzed was manually selected and segmented (Fig. 3(B), colormap) using the temporal mean intensity map of the hemoglobin-based parameter. This ensured that the observed effective changes occurring only on the tail of the mouse, excluding the O-cuff and background.

From the segmented tail region, a 4×4-pixel region of interest (ROI) was selected using the $[\Delta HbO]$ based maps as a reference (Fig. 3(B), black and white squares). The ROI was manually selected by the researcher within the tail region with an intensity value close to maximum of $[\Delta HbO]$ (Fig. 3(B)). The extracted trendlines of the dynamically changing hemoglobin-based parameters ($[\Delta HbO]$, $[\Delta HbR]$ and $[\Delta HbT]$) were averaged across the 16 pixels of the ROI (Fig. 3(C)).

The time-varying hemoglobin-based parameters were initialized and normalized with respect to a chosen timepoint during the rest period ($[\Delta HbO_0]$, $[\Delta HbR_0]$, $[\Delta HbT_0]$), 60 seconds prior to the first occlusion cycle (Eq. 7–9, Fig. 3(D)). ROI extraction was completed thrice per imaging session for each mouse to evaluate the manual ROI selection variance. All subsequent analyses within this study were based on the three selected ROI's.

$$[\Delta HbO_{norm}](x,y,t) = \frac{[\Delta HbO](x,y,t) - [\Delta HbO_0](x,y,0)}{[\Delta HbO_0](x,y,0)} \tag{7}$$

$$[\Delta HbR_{norm}](x,y,t) = \frac{[\Delta HbR](x,y,t) - [\Delta HbR_0](x,y,0)}{[\Delta HbR_0](x,y,0)} \tag{8}$$

$$[\Delta HbT_{norm}](x,y,t) = \frac{[\Delta HbT](x,y,t) - [\Delta HbT_0](x,y,0)}{[\Delta HbT_0](x,y,0)} \tag{9}$$

2.4.2. Study 1: rate of change in hemoglobin-based parameters during occlusion (occlusion slope)

The rate of change in hemoglobin-based parameters during the first occlusion cycle (or the occlusion slope) was calculated using the time-varying normalized parameters ($[\Delta HbO_{norm}]$, $[\Delta HbR_{norm}]$, and $[\Delta HbT_{norm}]$) as shown in Eq. 5–7, respectively, from the selected ROIs. Based on the specified CODA monitor occlusion time (10-12 seconds), the occlusion slope was calculated based on the response time (time until half of maximum pressure is reached); hence, the first 6 seconds were utilized [23]. The rate of change in terms of each of the hemoglobin-based parameters for the three ROIs were calculated and averaged to represent the occlusion slope of each individual mouse (three-regions per mouse averaged) and the variance of subjective ROI selection was obtained using the standard error across the three-regions. Each average of the three-regions per mouse was used to calculate the group (pooled) mean of the CKD and CKD + VC groups and the occlusion slopes at W6, W9, and W12 were compared to determine if there are differences between the groups.

2.4.3. Study 2: extent of change in hemoglobin-based parameters during reperfusion

The extent of change in hemoglobin-based parameters during the reperfusion (after the first occlusion cycle) was calculated using the normalized parameters ($[\Delta HbO_{norm}]$, $[\Delta HbR_{norm}]$, and $[\Delta HbT_{norm}]$) as given in Eq. 10–12, respectively. The maximum and minimum peak values were based on the hemodynamic response of the first occlusion cycle in each session.

$$Extent\ of\ change\ in\ [\Delta HbO_{norm}] = [\Delta HbO_{norm}]_{max} - [\Delta HbO_{norm}]_{min} \tag{10}$$

$$Extent\ of\ change\ in\ [\Delta HbR_{norm}] = [\Delta HbR_{norm}]_{max} - [\Delta HbR_{norm}]_{min} \tag{11}$$

$$Extent\ of\ change\ in\ [\Delta HbT_{norm}] = [\Delta HbT_{norm}]_{max} - [\Delta HbT_{norm}]_{min} \tag{12}$$

The extent of change in the hemoglobin-based parameters for the three ROIs was identified and averaged to represent the drop or increase during the reperfusion stage of the first occlusion cycle. The pooled mean was calculated based on each three-region mouse average, like that in Study 1.

Biomedical Optics EXPRESS

2.5. Statistical analysis

Statistical evaluation of the VC effect on changes in hemoglobin-based parameters in response to the occlusion cycle was performed using paired one-tailed sample t-test. The analysis was performed across the weeks (W6, W9, and W12) within each group (CKD and CKD + VC) using the averaged hemoglobin-based parameters (as described in Sections 2.4.2 and 2.4.3).

It was hypothesized that the calcification presence would result in reduced hemoglobin changes due to the occlusion; thus, a one-tailed t-test was used in this study. A Holm-Bonferroni significance test ($\alpha = 0.1$) was applied for multiple week comparisons (W6 to W9, W9 to W12 and W6 to W12).

3. Results

3.1. Changes in hemoglobin-based parameter in mouse groups across weeks:

Trendlines for the effective hemoglobin-based parameters were normalized (with respect to 60s prior to occlusion, as described in section 2.4.1) and plotted per mouse to compare the changes across weeks. An example of the hemoglobin-based parameter trendlines for a CKD and a CKD + VC mouse can be visualized in Fig. 4. Initial 60 seconds (no occlusion, mouse at rest) are within the mouse-stabilization period prior to occlusion, while the following 30 seconds include the first occlusion cycle. The $[\Delta HbO]$, $[\Delta HbR]$ and $[\Delta HbT]$ trendlines correlated with a response to the occlusion stimulus from the CODA device, as observed in our prior studies [17]. A qualitative comparison across weeks showed a clear drop in the trendlines of three hemoglobin-based parameters ($[\Delta HbO]$, $[\Delta HbR]$ and $[\Delta HbT]$) from W6 to W12 in the CKD + VC group (Fig. 4(B),(D),(F),(H)). These trendlines showed no change in response to the occlusion by W12 (dark green, solid line in Fig. 4(B),(D),(F),(H)), as seen by a steeper slope at W6 (light green, dashed line in Fig. 4(B),(D),(F),(H)). On the contrary to the CKD + VC group, the trendlines for the same three hemoglobin-based parameters were similar between W6 and W12 but increased for W9 in the CKD group (Fig. 4(A),(C),(E),(G)). Unlike the trendlines in terms of $[\Delta HbO]$, $[\Delta HbR]$ and $[\Delta HbT]$, the trendlines in terms of $[\Delta StO_2]$ did not show any response to occlusion across all the weeks and in both the mouse groups. Both the mouse groups were on the same diet at W6, and hence the differentiation at W12 was quantified (for all hemoglobin-based parameters except $[\Delta StO_2]$) to further examine the effect of VC.

3.2. Rate of change of hemoglobin-based parameters during occlusion

A quantitative assessment of the hemoglobin-based parameters was conducted to compare the rate of change in these parameters in response to occlusion across all the three weeks (W6, W9 and W12) within each group. A linear regression analysis of the normalized hemoglobin-based parameters until the response time (initiation of the occlusion cycle until half the time to full occlusion, ~6s), was performed to calculate the rate of change. The rate of change in response to occlusion was analyzed within each group and for each of the hemoglobin-based parameters, as shown by bar plots in Fig. 5. The same analysis carried out for each individual mouse within the group is given in the Supplemental Material (Fig. S1). We observed a decreasing trend in the rate of change in all the hemoglobin-based parameters across the weeks in the CKD + VC group (Fig. 5(B),(D),(F)). This was not as apparent in the CKD group (Fig. 5(A),(C),(E))). Additionally, the standard error in the rate of change values across all weeks was higher in the CKD group, unlike the CKD + VC group.

A one-tailed paired t-test was performed to determine whether there were significant changes in the rate of change in the hemoglobin-based parameters in response to occlusion across the weeks (Table 1) and within each group. A significant change in $[\Delta HbO]$ was found in the CKD + VC group between W6 to W12 and W9 to W12 (Table 1(A) and Fig. 5(B)). When comparing the rate of change during occlusion based on total hemoglobin, the significant change was only seen

Biomedical Optics EXPRESS

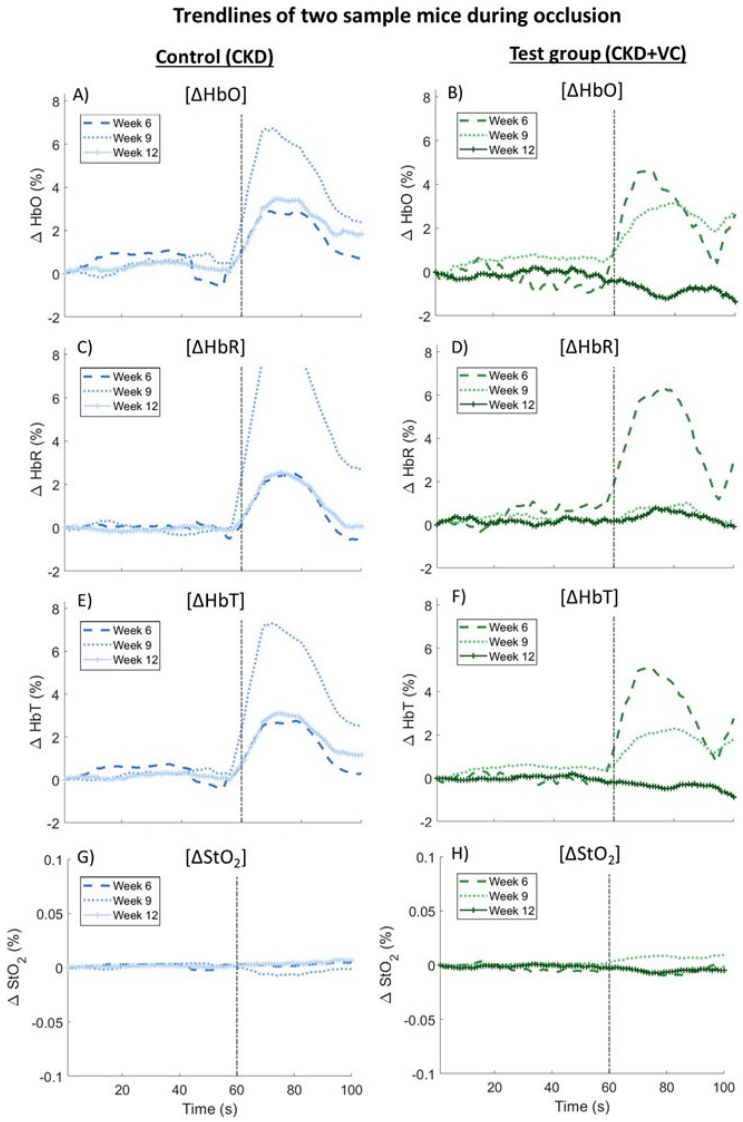

Fig. 4. Hemoglobin-based parameter trendlines in terms of A,B) [ΔHbO] C,D) [ΔHbR], E,F) [ΔHbT], and G,H) [ΔStO_2] normalized with respect to rest period of mouse at timepoint 60s prior to occlusion, for both the mice groups (CKD and CKD + VC), and across weeks 6, 9 and 12. The dashed vertical in each plot at timepoint 60s depicts the onset of the occlusion stimulus.

Biomedical Optics EXPRESS

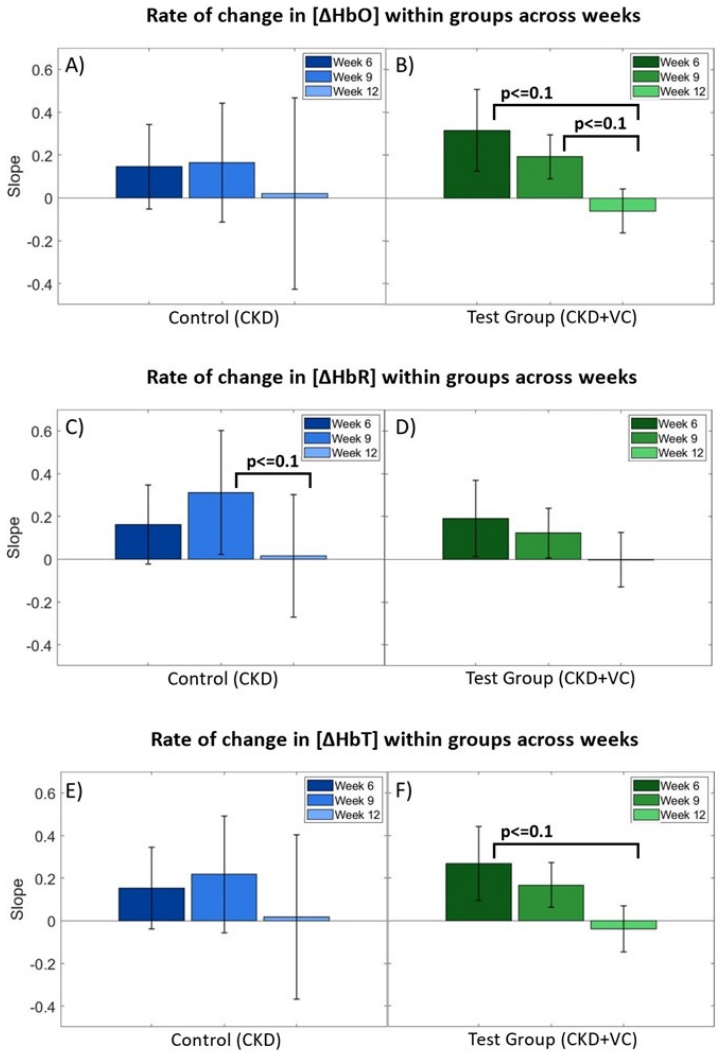

Fig. 5. Comparison of the rate of change during occlusion of hemoglobin-based parameters in response to an occlusion stimulus across the two groups (CKD and CKD + VC) and weeks. Mean of the three-region averages (pooled mean) ± standard error per group for W6, W9 and to W12 shown for each of the hemoglobin-based parameter- A),B) *[ΔHbO]*; C),D) *[ΔHbR]*; and E), F) [*ΔHbT*]. Number of mice for the CKD group was n = 6 and for the CKD + VC group n = 5.

Biomedical Optics EXPRESS

between W6 to W12 in the CKD + VC group (Table 1(C) and Fig. 5(F)). On the contrary, rate of change during occlusion based on [ΔHbR] was not significant across the weeks in CKD + VC group (Table 1(B) and Fig. 5(D)). Interestingly the rate of change based on [ΔHbR] was significant between W9 to W12 in the CKD group (Table 1(B) and Fig. 5(C)), in spite of a large standard error across the weeks (Fig. 5(A),(C),(E)).

Table 1. Rate of change during occlusion in all three hemoglobin-based parameters (one-tailed paired sample t-tests) between the weeks and within the groups. A Holm-Bonferroni correction was completed for each mice group separately. *Significant with $\alpha = 0.1$. The cases with $p \leq 0.1$ are given with an asterisk and shaded in grey.

A) [ΔHbO]: Rate of change during occlusion	**CKD**		**CKD+VC**	
	t-statistic	**p-value**	**t-statistic**	**p-value**
W6 vs. W9	-1.079	0.495	1.491	0.315
W9 vs. W12	1.553	0.272	3.055	**0.056***
W6 vs. W12	0.987	0.554	3.565	**0.035***

B) [ΔHbR]: Rate of change during occlusion	**CKD**		**CKD+VC**	
	t-statistic	**p-value**	**t-statistic**	**p-value**
W6 vs. W9	-2.091	0.136	0.689	0.793
W9 vs. W12	2.633	**0.070***	1.408	0.347
W6 vs. W12	1.289	0.381	2.071	0.161

C) [ΔHbT]: Rate of change during occlusion	**CKD**		**CKD+VC**	
	t-statistic	**p-value**	**t-statistic**	**p-value**
W6 vs. W9	-1.510	0.282	1.260	0.411
W9 vs. W12	2.000	0.150	2.430	0.105
W6 vs. W12	1.120	0.468	3.280	**0.045***

3.3. Extent of change in hemoglobin-based parameters

A second quantitative assessment of the hemoglobin-based parameters was conducted to compare the extent of change in these parameters in response to occlusion across all the three weeks (W6, W9 and W12) within each group. The pooled mean was calculated for each mouse using the three-ROI average per mouse for all hemoglobin-based parameters. The extent of change in response to occlusion was analyzed within each group and for each of the hemoglobin-based parameters, as shown by bar plots in Fig. 6. The same analysis carried out for each individual mouse within the group is given in Supplemental Material (Fig. S2). The individual assessment of each mouse at each imaging session permitted the identification of possible outliers.

A decreasing trend for the extent of change in all the hemoglobin-based parameters was observed in the CKD + VC group (Fig. 6(B),(D),(F)), unlike the CKD group (Fig. 6(A),(C),(E)) The standard error for the extent of change in these parameters across all weeks was higher in the CKD as well as the CKD + VC group.

Biomedical Optics EXPRESS

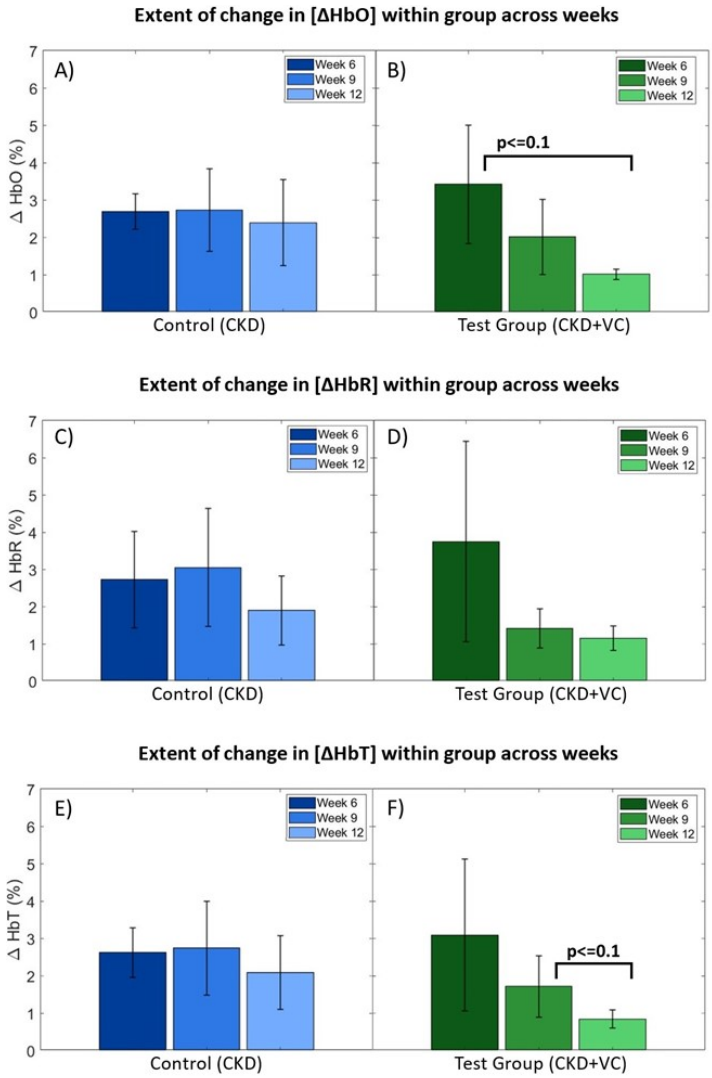

Fig. 6. Comparison of the extent of change of hemoglobin-based parameters in response to an occlusion stimulus across the two groups (CKD and CKD + VC) and weeks. Mean of the three-region averages (pooled mean) ± standard error per group for W6, W9 and to W12 shown for each of the hemoglobin-based parameter- A),B) [*ΔHbO*]; C),D) [*ΔHbR*]; and E), F) [*ΔHbT*]. For CKD group n = 6 and for CKD + VC group n = 5

Biomedical Optics EXPRESS

A one-tailed paired t-test was performed to determine whether there were significant changes in the extent of change in the hemoglobin-based parameters in response to occlusion across the weeks (Table 2) and within each group. A significant change was noticed for the CKD + VC in extent of change in [ΔHbO] from W6 to W12 and [ΔHbT] from W9 to W12 (Table 2(A),(C)). There was no significant change in extent of change in [ΔHbR] based parameters across the weeks in either mice group (Table 2(B)).

Table 2. Extent of change in all three hemoglobin-based parameters (one-tailed paired sample t-tests) between the weeks and within the groups. A Holm-Bonferroni correction was completed for each mice group separately. *Significant with $\alpha = 0.1$. The cases with $p \leq 0.1$ are given with an asterisk and shaded in grey.

A) [ΔHbO]: Extent of change during occlusion	**CKD**		**CKD+VC**	
	t-statistic	**p-value**	**t-statistic**	**p-value**
W6 vs. W9	-0.088	1.400	1.911	0.193
W9 vs. W12	0.420	1.038	2.242	0.133
W6 vs. W12	0.536	0.922	3.169	**0.051***

B) [ΔHbR]: Extent of change during occlusion	**CKD**		**CKD+VC**	
	t-statistic	**p-value**	**t-statistic**	**p-value**
W6 vs. W9	-0.372	1.087	2.023	0.170
W9 vs. W12	1.482	0.298	1.330	0.381
W6 vs. W12	1.518	0.284	2.018	0.171

C) [ΔHbT]: Extent of change during occlusion	**CKD**		**CKD+VC**	
	t-statistic	**p-value**	**t-statistic**	**p-value**
W6 vs. W9	-0.188	1.284	1.547	0.294
W9 vs. W12	0.824	0.669	2.616	**0.087***
W6 vs. W12	1.030	0.522	2.320	0.120

A one-tailed paired t-test was performed to determine whether there were significant changes in the hemoglobin-based parameters across the weeks (Table 1). A significant change in [ΔHbO] was found in the CKD + VC group between W6 to W12 (Table 2(A) and Fig. 6(B)). When comparing the extent of change during occlusion based on total hemoglobin, a significant change was seen between W9 to W12 in the CKD + VC group (Table 2(C) and Fig. 6(F)). On the contrary, rate of change during occlusion based on all three hemoglobin-based parameters was not significant across the weeks in the CKD group (Table 2 and Fig. 6(A),(C),(E)).

3.4. Weight change across disease development

The weight of the mice was monitored across the study to evaluate dietary effects on each group. Mice from both groups had weight loss from W0 to W6 (Fig. 7(A),(B)). The CKD mice had a distinct loss across the 12 weeks. On the other hand, CKD + VC mice noticed an initial decrease (W0 to W6) but stabilized once the 1.8% high phosphate diet was introduced at W6 (Fig. 7).

Biomedical Optics EXPRESS

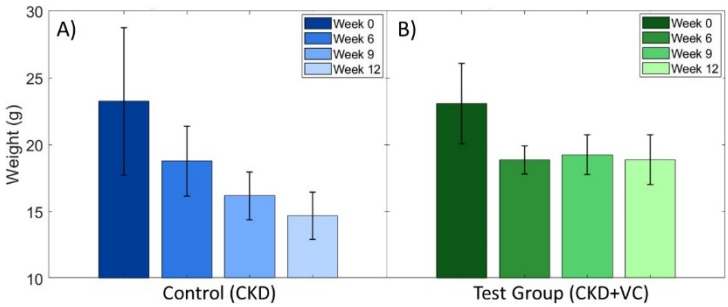

Fig. 7. Weight changes from W0 to W12 are shown as average weight and standard deviation across both groups (CKD and CKD + VC). Both groups were placed on a 0.2% adenine and 0.6% phosphate diet from W0 to W12. The CKD + VC group was supplemented with a 1.8% high phosphate diet from W6 onwards.

4. Discussion

CVD is the leading cause of death in CKD patients and the presence of vascular calcification is the most significant predictor of cardiovascular morbidity and mortality [1,2]. Our data suggests that blood flow changes with an occlusion stimulus can act as a biomarker of VC. In this study, we obtained dynamic NIRS measurements in response to a vascular occlusion stimulus and monitored changes in the hemoglobin-based parameters throughout disease progression in a mouse model of CKD-induced VC. This is a novel technique that can analyze blood flow on the peripheries to identify the presence of VC. Current techniques to assess VC require expensive imaging modalities that are not well-suited for regular monitoring nor low resource settings, which could be mitigated with this technique.

In this study, the onset of VC occurred with the high phosphate diet that was introduced during W6 to the CKD + VC mice group. Extensive studies in the past have reported that the high phosphate diet induces VC in mice [19,20,24]. Maintaining the high adenine diet without the elevated phosphate for the entire 12 weeks (CKD group) sustained kidney damage but did not lead to vascular calcification [19,22]. The principal finding of this study is that the presence of induced VC can be distinguished by analyzing hemodynamic response from the peripheries using NIRS-based imaging and a vascular occlusion test (VOT). Initial observation of the vascular occlusion effect on $[\Delta HbT]$ over time showed a qualitative decrease as calcification developed in the CKD + VC group (Fig. 4). As the tail was occluded to maximum pressure (10-12s from the onset of occlusion at timepoint 60s), there was an increase in $[\Delta HbT]$ followed by a plateau consistent with a total occlusion (Fig. 4(E)-(F)) [25]. The increased $[\Delta HbT]$ occurs as venous flow becomes restricted, and blood accumulates from the arterial side. Once both arterial inflow and venous outflow become constricted, $[\Delta HbT]$ plateaus as blood can no longer enter nor leave the local circulation. A similar trend was observed in $[\Delta HbO]$ and $[\Delta HbR]$ in response to the vascular occlusion effect (Fig. 4(A)-(D)). This trend of increasing concentrations of all three hemoglobin-based parameters in response to occlusion is typically observed during venous occlusion and total occlusion [22]. However, since the maximum occlusion pressure applied during the study was 250 mmHg, a total occlusion of both arterial and venous flow is assumed. CKD + VC mice exhibited an increased $[\Delta HbT]$ trendline during occlusion at W6 (Fig. 4(F)); however, the effect was reduced by W9 and nearly no effect by W12. A similar reduction in the overall change in $[\Delta HbO]$ and $[\Delta HbR]$ in response to occlusion was distinctly observed at W9 and W12 in the CKD + VC group (Fig. 4(B),(D)). The diminished response to the occlusion at W9 and W12, following the onset of VC could possibly be from stiffened vascular walls that do not respond to the constriction in the test group (CKD + VC). Our future studies will

Biomedical Optics EXPRESS

involve correlation of the peripheral hemodynamic response to occlusion with Doppler-based assessments of blood flow and changes in vascular biomechanics due to VC.

Hemodynamic response in terms of $[\Delta StO_2]$ did not show any distinct increase or decrease in response to occlusion in both the mice groups and across all the weeks (Fig. 4(G)-(H)). This is probably due a short occlusion time (< 3 sec) and the maximum pressure of 250 mmHg, both of which may have been insufficient to observe changes during occluded time. In a prior study on rabbits, these small animals demonstrated that a VOT with an occlusion of 120 seconds causes changes in $[HbO]$, $[HbR]$, and $[HbT]$ [25]. A change in $[StO_2]$ was also observed due to the increased occlusion time (s) at the chosen peak pressures to allow venous, arterial, and total occlusion [22]. A VOT study involving humans has an occlusion protocol of 3 minutes causing a large decrease in oxygen saturation [26]. If the occlusion time at maximum pressure was extended to 2-3 minutes in our study, a change in $[\Delta StO_2]$ would have been possible. A typical C57BL/6J mouse has a systolic pressure of $120 \pm 2\ mmHg$, and diastolic pressure of $99 \pm 2 mmHg$ [27], similar to that in humans. A previous study using the same diet regimen and duration showed that the CKD + VC mice showed lower systolic and diastolic blood pressures when compared to CKD mice [22]. In CKD patients, the presence of VC has a significant prognostic value – CKD patients with coexistence of VC and hypotension have more cardiovascular events [28]. This further warrants the need for a tool that can easily and accurately detect VC in CKD patients.

In our study, a KENT CODA device was used to perform systematic vascular occlusions on the mouse tail. However, the device was limited to a pre-set occlusion time of <3s at the maximum pressure of 250 mmHg. The lack of extensive occlusion to cause a hypoxic condition and a related drop in oxygen saturation could have resulted in a no distinct change in $[\Delta StO_2]$ in our current study. However, this occlusion time was probably sufficient to show a distinct change in the other three hemoglobin-based parameters as described above and given in Fig. 4. Currently, studies are ongoing to develop an -in-house blood pressure cuff for small animal studies that is adaptable to various occlusion rates and times during imaging studies. Control of the occlusion parameters would allow a VOT protocol in the mice similar to that in humans and could be analyzed for vascular calcification effects on peripheral tissue oxygenation.

A quantitative assessment of the three hemoglobin-based parameters ($[\Delta HbO]$, $[\Delta HbR]$, $[\Delta HbT]$) for all mice within the study involved analyzing the rate of change in each of these parameters during occlusion (occlusion slope at half-max). The rate of change during occlusion was slightly variable among the mice due to the limitations in the CODA device that cannot control the vascular occluding time. Despite the variability between each CKD + VC mouse, there was an overall decreasing trend in the CKD + VC group across the weeks in terms of the rate of change during occlusion for the three hemoglobin-based parameters (Fig. 5). Similarly, the extent of change in all three hemoglobin-based parameters showed a decreasing trend for the CKD + VC group across the weeks.

The reduction in the rate of change and extent of change in the hemoglobin-based parameters during occlusion of the CKD + VC group at W12 possibly occurs because the stiffened vascular walls do not respond to the constriction during VOT. We can use these two quantitative measures to statistically determine if there are differences between the presence or absence of vascular occlusion (i.e. difference between CKD + VC and CKD mouse groups), as observed by the difference in the rate of change in ($[\Delta HbO]$) during occlusion between W6 to W12 and W9 to W12. The current study is a pilot study with a small number of mice per group. Extensive work is yet to be performed on a larger cohort of mice and using our in-house custom blood pressure cuff that allows modifications in the VOT protocol and perform systematic studies. Results from future extensive studies could further validate the technique for VC detection in CKD by ensuring that the changes are also observed in a larger population.

Chronic kidney disease has secondary effects on muscle mass and weight [29], with the latter observed in our groups (CKD) throughout the study (Fig. 7(A)). Despite the test group

Biomedical Optics EXPRESS

(CKD + VC) receiving the high adenine, CKD-inducing diet throughout the study, it seems that the supplemental high phosphate prompted a stabilization in weight (Fig. 7(B)). Vasculature affected by calcifications has been shown to have negative effects on the oxygenation reaching the tissue within the area [30]. Tissue oxygenation can be affected by changes in blood volume, which can occur due to fluctuations in weight. Significant changes in $[\Delta HbO]$ and $[\Delta HbT]$ were observed even when the CKD + VC group weight was stabilized and did not significantly drop throughout the experiment. Therefore, we hypothesize that the hemoglobin-based parameter changes observed are not caused by the reduced body weight in this study.

The current study correlated the onset of aortic VC to peripheral hemodynamic changes in response to occlusion. The onset of aortic VC may have affected the extent of calcification in the peripheral arteries to cause a difference in the hemodynamic response during peripheral vascular imaging. However, the correlation between aortic VC, the extent of calcification in the peripheral arteries, and the hemodynamic changes in the peripheral tail region is yet to be determined and is a focus of our future work. Understanding this correlation will lay the foundation to determine if the proposed technique of peripheral hemodynamic response to occlusion is a viable approach to predict the onset of aortic VC, peripheral calcification, or both.

5. Conclusions

An in-house NIR-based optical imaging device (or NIROS) was used to acquire spatio-temporal hemodynamic images of mice that developed CKD with (CKD + VC group) and without (CKD group) VC. An occlusion stimulus was applied to evaluate the changes in hemoglobin-based parameters in the tail and identify the presence of VC. The statistical analysis demonstrated that $[\Delta HbO]$ and $[\Delta HbT]$ are the two hemoglobin-based parameters that were significantly different in their rate of change and extent of change in response to the occlusion for the CKD + VC group. And more specifically, the rate of change in $[\Delta HbO]$ differentiated between W6 to W12 as well as W9 to W12. This possibly implies that rate of change in $[\Delta HbO]$ could be a potential indicator for determining the presence of VC.

Peripheral hemoglobin-based parameters' responses to an occlusion stimulus with the onset of VC should be furthered studied, as this study showed the potential of using NIRS-based measurements as an indicator of VC. Future work should be performed on a larger cohort of small animals using various occlusion protocols to identify a robust hemoglobin-based biomarker that can predict the presence as well as the degree of vascular calcification.

Funding. National Institute of Diabetes and Digestive and Kidney Diseases (F31DK125153, F31HL154671); National Heart, Lung, and Blood Institute (1R01HL160740); National Science Foundation (ERC PATHS-UP 1648451); Florida International University (BME Coulter Seed Grant, Coulter Undergraduate Research Experience).

Acknowledgements. The authors would like to acknowledge the funding sources.

Disclosures. The authors declare no conflicts of interest.

Data availability. Data underlying the results presented in this paper are not publicly available at this time but may be obtained from the authors upon reasonable request.

Supplemental document. See Supplement 1 for supporting content.

References

1. K. L. Johansen, G. M. Chertow, R. N. Foley, *et al.*, "US Renal Data System 2020 Annual Data Report: Epidemiology of Kidney Disease in the United States," Am. J. Kidney Dis. **77**(4), A7–A8 (2021).
2. G. M. London, A. P. Guérin, S. J. Marchais, F. Métivier, B. Pannier, and H. Adda, "Arterial media calcification in end-stage renal disease: Impact on all-cause and cardiovascular mortality," Nephrol., Dial., Transplant. **18**(9), 1731–1740 (2003).
3. A. L. Durham, M. Y. Speer, M. Scatena, C. M. Giachelli, and C. M. Shanahan, "Role of smooth muscle cells in vascular calcification: Implications in atherosclerosis and arterial stiffness," Cardiovasc Res **114**(4), 590–600 (2018).
4. S. L. Cheng, A. Behrmann, J. S. Shao, B. Ramachandran, K. Krchma, Y. B. Arredondo, A. Kovacs, M. Mead, R. Maxson, and D. A. Towler, "Targeted reduction of vascular Msx1 and Msx2 mitigates arteriosclerotic calcification and aortic stiffness in LDLR-deficient mice fed diabetogenic diets," Diabetes **63**(12), 4326–4337 (2014).

Biomedical Optics EXPRESS

5. J. D. Hutcheson, C. Goettsch, M. A. Rogers, and E. Aikawa, "Revisiting cardiovascular calcification: A multifaceted disease requiring a multidisciplinary approach," Semin. Cell Dev. Biol. **46**, 68–77 (2015).
6. J. P. Roijers, Y. S. Rakké, C. J. Hopmans, M. G. Buimer, G. H. Ho, H. G. W. de Groot, E. J. Veen, P. G. H. Mulder, and L. van der Laan, "A mortality prediction model for elderly patients with critical limb ischemia," J Vasc Surg **71**(6), 2065–2072.e2 (2020).
7. C. L. Huang, I. H. Wu, Y. W. Wu, J. J. Hwang, S. S. Wang, W. J. Chen, W. J. Lee, and W. S. Yang, "Association of lower extremity arterial calcification with amputation and mortality in patients with symptomatic peripheral artery disease," PLoS One **9**(2), e90201 (2014).
8. S. Arya, Z. Binney, A. Khakharia, L. P. Brewster, P. Goodney, R. Patzer, J. Hockenberry, and P. W. F. Wilson, "Race and socioeconomic status independently affect risk of major amputation in peripheral artery disease," J. Am. Heart Assoc. **7**(2), e007425 (2018).
9. M. Cai, Y. Xie, B. Bowe, A. K. Gibson, M. A. Zayed, T. Li, and Z. Al-Aly, "Temporal Trends in Incidence Rates of Lower Extremity Amputation and Associated Risk Factors among Patients Using Veterans Health Administration Services from 2008 to 2018," JAMA Netw Open **4**(1), e2033953 (2021).
10. S. Vemulapalli, M. A. Greiner, W. S. Jones, M. R. Patel, A. F. Hernandez, and L. H. Curtis, "Peripheral arterial testing before lower extremity amputation among medicare beneficiaries, 2000 to 2010," Circ Cardiovasc Qual Outcomes **7**(1), 142–150 (2014).
11. P. Raggi, A. Bellasi, D. Bushinsky, J. Bover, M. Rodriguez, M. Ketteler, S. Sinha, C. Salcedo, K. Gillotti, C. Padgett, R. Garg, A. Gold, J. Perelló, and G. M. Chertow, "Slowing progression of cardiovascular calcification with snf472 in patients on hemodialysis: Results of a randomized phase 2b study," Circulation **141**(9), 798 (2020).
12. N. M. Lioufas, E. Pedagogos, C. M. Hawley, E. M. Pascoe, G. J. Elder, S. V. Badve, A. Valks, and N. D. Toussaint, "Aortic Calcification and Arterial Stiffness Burden in a Chronic Kidney Disease Cohort with High Cardiovascular Risk: Baseline Characteristics of the Impact of Phosphate Reduction On Vascular End-Points in Chronic Kidney Disease Trial," Am. J. Nephrol. **51**(3), 201–215 (2020).
13. R. Smith-Bindman, M. L. Kwan, E. C. Marlow, M. K. Theis, W. Bolch, S. Y. Cheng, E. J. A. Bowles, J. R. Duncan, R. T. Greenlee, L. H. Kushi, J. D. Pole, A. K. Rahm, N. K. Stout, S. Weinmann, and D. L. Miglioretti, "Trends in Use of Medical Imaging in US Health Care Systems and in Ontario, Canada, 2000-2016," JAMA - Journal of the American Medical Association **322**(9), 843 (2019).
14. K. M. Lefebvre and J. Chevan, "The persistence of gender and racial disparities in vascular lower extremity amputation: An examination of HCUP-NIS data (2002-2011)," Vascular Medicine (United Kingdom) **20**(1), 51 (2015).
15. K. F. Ma, S. F. Kleiss, R. C. L. Schuurmann, R. P. H. Bokkers, Ç. Ünlü, and J. P. P. M. De Vries, "A systematic review of diagnostic techniques to determine tissue perfusion in patients with peripheral arterial disease," Expert Rev. Med. Devices **16**(8), 697–710 (2019).
16. K. Leiva, J. Mahadevan, K. Kaile, R. Schutzman, E. Robledo, S. Narayanan, V. Muthukrishnan, V. Mohan, W. Wu, and A. Godavarty, "Breath-Hold Paradigm to Assess Variations in Oxygen Flow in Diabetic Foot Ulcers Using a Noncontact Near-Infrared Optical Scanner," Adv Wound Care (New Rochelle) **8**(8), 386–402 (2019).
17. K. Leiva, D. Leizaola, I. Gonzalez, V. Dargam, H. Alirezaei, K. Kaile, E. Robledo, J. Hutcheson, and A. Godavarty, "Spatial–Temporal Oxygenation Mapping Using a Near-Infrared Optical Scanner: Towards Peripheral Vascular Imaging," Ann. Biomed. Eng. **51**(9), 2035–2047 (2023).
18. T. Baltrūnas, V. Mosenko, A. Mackevičius, V. Dambrauskas, I. Ašakienė, K. Ručinskas, and P. Narmontas, "The use of near-infrared spectroscopy in the diagnosis of peripheral artery disease: A systematic review," Vascular **30**(4), 715–727 (2022).
19. T. Tani, H. Orimo, A. Shimizu, and S. Tsuruoka, "Development of a novel chronic kidney disease mouse model to evaluate the progression of hyperphosphatemia and associated mineral bone disease," Sci. Rep. **7**(1), 2233 (2017).
20. A. Bakhshian Nik, H. H. Ng, S. K. Ashbrook, P. Sun, F. Iacoviello, P. R. Shearing, S. Bertazzo, D. Mero, B. B. Khomtchouk, and J. D. Hutcheson, "Epidermal Growth Factor Receptor Inhibition Prevents Vascular Calcifying Extracellular Vesicle Biogenesis," American Journal of Physiology-Heart and Circulatory Physiology **324**(4), H553–H570 (2023).
21. R. Kwasinski, C. Fernandez, K. Leiva, R. Schutzman, E. Robledo, P. Kallis, L. J. Borda, R. Kirsner, F. Perez-Clavijo, and A. Godavarty, "Tissue Oxygenation Changes to Assess Healing in Venous Leg Ulcers Using Near-Infrared Optical Imaging," Adv Wound Care (New Rochelle) **8**(11), 565–579 (2019).
22. V. Dargam, H. H. Ng, S. Nasim, D. Chaparro, C. I. Irion, S. R. Seshadri, A. Barreto, Z. C. Danziger, L. A. Shehadeh, and J. D. Hutcheson, "S2 Heart Sound Detects Aortic Valve Calcification Independent of Hemodynamic Changes in Mice," Front. Cardiovasc. Med. **9**, 809301 (2022).
23. C.-W. Sun and C.-C. Chuang, "Hemodynamics Study Based on Near-Infrared Optical Assessment," in *Hemodynamics - New Diagnostic and Therapeutic Approaches* (2012).
24. S. K. Ashbrook, A. M. Valentin Cabrera, M. Shaver, and J. D. Hutcheson, "Analysis of Extracellular Vesicle-Mediated Vascular Calcification Using In Vitro and In Vivo Models," J. Visualized Exp. **2023**(191), (2023).
25. M. S. Irwin, M. S. Thorniley, C. J. Doré, and C. J. Green, "Near infra-red spectroscopy: a non-invasive monitor of perfusion and oxygenation within the microcirculation of limbs and flaps," Br. J. Plast. Surg. **48**(1), 14–22 (1995).
26. R. Bezemer, A. Lima, D. Myers, E. Klijn, M. Heger, P. T. Goedhart, J. Bakker, and C. Ince, "Assessment of tissue oxygen saturation during a vascular occlusion test using near-infrared spectroscopy: the role of probe spacing and measurement site studied in healthy volunteers," Crit Care **13**(Suppl 5), S4 (2009).

Biomedical Optics EXPRESS

27. D. L. Mattson, "Comparison of arterial blood pressure in different strains of mice," Am J Hypertens **14**(5), 405–408 (2001).
28. J. S. Kim and H. S. Hwang, "Vascular calcification in chronic kidney disease: Distinct features of pathogenesis and clinical implication," Korean Circ J **51**(12), 961 (2021).
29. R. H. Mak, A. T. Ikizler, C. P. Kovesdy, D. S. Raj, P. Stenvinkel, and K. Kalantar-Zadeh, "Wasting in chronic kidney disease," J Cachexia Sarcopenia Muscle **2**(1), 9–25 (2011).
30. M. Wu, C. Rementer, and C. M. Giachelli, "Vascular calcification: An update on mechanisms and challenges in treatment," Calcif Tissue Int **93**(4), 365–373 (2013).